

Exploiting Defenses against GAN-Based Feature Inference Attacks in Federated Learning

XINJIAN LUO, National University of Singapore, Singapore

XIANGLONG ZHANG, University of Science and Technology Beijing, China

Federated learning (FL) is a decentralized model training framework that aims to merge isolated data islands while maintaining data privacy. However, recent studies have revealed that Generative Adversarial Network (GAN) based attacks can be employed in FL to learn the distribution of private datasets and reconstruct recognizable images. In this paper, we exploit defenses against GAN-based attacks in FL and propose a framework, Anti-GAN, to prevent attackers from learning the real distribution of the victim's data. The core idea of Anti-GAN is to manipulate the visual features of private training images to make them indistinguishable to human eyes even restored by attackers. Specifically, Anti-GAN projects the private dataset onto a GAN's generator and combines the generated fake images with the actual images to create the training dataset, which is then used for federated model training. The experimental results demonstrate that Anti-GAN is effective in preventing attackers from learning the distribution of private images while causing minimal harm to the accuracy of the federated model.

CCS Concepts: • **Security and privacy** → *Distributed systems security*.

Additional Key Words and Phrases: Defense, Feature Inference, GAN, Federated Learning

ACM Reference Format:

Xinjian Luo and Xianglong Zhang. 2018. Exploiting Defenses against GAN-Based Feature Inference Attacks in Federated Learning. *J. ACM* 37, 4, Article 111 (August 2018), 23 pages. <https://doi.org/XXXXXX.XXXXXXX>

1 INTRODUCTION

Machine Learning (ML), particularly deep learning, has gained widespread adoption in various real-life applications, such as face recognition and robotics, owing to its impressive performance. However, ML algorithms are susceptible to different types of attacks, such as model inversion [9, 68] and membership inference [42, 46], which can jeopardize user privacy and lead to unintended information leakage. To overcome these challenges, *federated learning* (FL) [34] has emerged as a promising solution, which enables collaborative model training between a central server and multiple clients while ensuring user-level privacy and reducing data fragmentation. Despite the advantages of FL, recent research has identified a new threat to its security: GAN-based feature inference attacks [17, 54]. In contrast to traditional feature inference attacks that exploit record-level privacy leakage to infer individual training images from trained models [30, 31, 36, 67], GAN-based attacks aim to infer the group-level information of private training images, i.e., the data distribution, which poses a significant challenge to existing privacy-preserving mechanisms such as differential privacy (DP) [60]. Although DP has been shown to be effective in preventing record-level privacy leakage in FL [46], protecting group-level information is not guaranteed by its

Authors' addresses: Xinjian Luo, National University of Singapore, Singapore, xinjian.luo@u.nus.edu; Xianglong Zhang, University of Science and Technology Beijing, China, xlzhang@ustb.edu.cn.

Permission to make digital or hard copies of all or part of this work for personal or classroom use is granted without fee provided that copies are not made or distributed for profit or commercial advantage and that copies bear this notice and the full citation on the first page. Copyrights for components of this work owned by others than the author(s) must be honored. Abstracting with credit is permitted. To copy otherwise, or republish, to post on servers or to redistribute to lists, requires prior specific permission and/or a fee. Request permissions from permissions@acm.org.

© 2018 Copyright held by the owner/author(s). Publication rights licensed to ACM.

ACM 0004-5411/2018/8-ART111

<https://doi.org/XXXXXX.XXXXXXX>

definition [24]. This highlights the need for developing novel privacy-preserving techniques that can safeguard group-level privacy in FL. However, despite its significance, the current research landscape has yet to adequately explore this issue. It is worth noting that the existing privacy-preserving mechanisms [11, 43] in FL are primarily designed to counteract record-level attacks [31, 69], and are insufficient in mitigating GAN-based attacks. Therefore, in this paper, we aim to address the vulnerability of FL to GAN-based attacks by developing a robust defense that is capable of mitigating the privacy risks posed by such attacks while effectively preserving the model utility.

There are three primary challenges to consider when designing defenses against GAN-based attacks in the context of FL. *First*, traditional cryptographic methods, such as homomorphic encryption [25, 57] and secure multiparty computation [4, 38], offer limited utility. The reason is that these methods require significant computational resources [49, 57, 64], thereby restricting their application scenarios. In addition, encrypting local gradients can inhibit anomaly detection methods designed to counteract poisoning-based attacks [3, 24]. *Second*, the effectiveness of noise injection, particularly techniques like DP [49, 60, 71], is limited in mitigating GAN-based attacks, as demonstrated in previous research [17]. While DP provides theoretical privacy guarantees for individual private images, GANs aim to reconstruct representations of specific classes [48, 58], surpassing the scope of DP's privacy guarantee. *Third*, the success of GAN-based attacks is closely tied to the practicality of the federated model and the memorization nature of neural network models [6]. In other words, defending against such attacks becomes challenging as long as the victim's local model maintains a sufficiently high classification accuracy [17].

It is worth noting that existing defense mechanisms, such as cryptographic methods and noise injection, primarily focus on safeguarding privacy during the training phase, but their effectiveness in mitigating GAN-based attacks is limited. Motivated by this observation, we shift our attention towards privacy protection in the data generation phase before model training and propose a defense mechanism called Anti-GAN to address these above challenges. The core idea underlying Anti-GAN is to generate training images using a GAN model, where the visual characteristics of the generated images are obfuscated through a carefully designed loss function. This approach ensures that the attacker's GAN model can only learn the distribution of visually indistinguishable images. However, as the distribution of the obfuscated images may differ from that of real images, this strategy could potentially result in a degradation of accuracy when the federated model is tested on real images. To overcome this issue, we devise a novel structure for the victim's GAN model, enabling effective preservation of the classification features from real images while reasonably corrupting the visual features of the generated images. To further enhance the performance of the federated model, we devise a modified Mixup [65] method to generate the final training images by mixing the generated fake images with the real images. It is important to note that Anti-GAN is specifically designed to obfuscate object details rather than the entire visual features of training images. Anti-GAN can preserve the semantic information necessary for the downstream classifier, such as the outline of a human face, while rendering object details, such as eyes and noses, indistinguishable to the human eye. Consequently, our scheme can significantly reduce the accuracy degradation caused to the federated model and ensure that images reconstructed by attackers are rendered useless.

The framework of Anti-GAN is depicted in Fig. 1. Particularly, the victim initiates the defense process by training a GAN model using the private dataset X , generating corresponding fake images X' . The objective is to ensure that X' and X possess similar classification features while obscuring the visual features of X' . Subsequently, the generated X' is mixed with X to form the training dataset \hat{X} , which is then used to train the federated model. To assess the effectiveness of Anti-GAN, we conducted extensive experiments utilizing the MNIST [61], FashionMNIST [59], and CelebA [29]

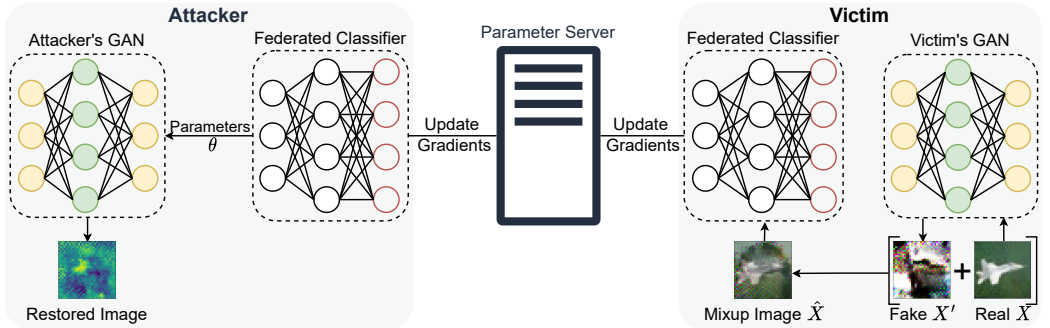


Fig. 1. The defense framework of Anti-GAN.

datasets. The results demonstrate that Anti-GAN successfully reduces the plausibility of images reconstructed by the attacker’s GAN model while having minimal impact on the accuracy of the global federated model. Our results also show that, beyond countering group-level GAN-based attacks, Anti-GAN can effectively mitigate record-level gradient-matching attacks [69] as well. Our contributions are summarized as follows:

- We explore the defenses against GAN-based feature inference attacks within the context of FL. The proposed defense framework, Anti-GAN, effectively thwarts the attacker’s ability to learn distinguishable private visual distribution from the victim’s local models.
- We introduce an unsupervised learning task to the victim’s GAN model, enabling the obfuscation of visual features in the generated images. We design a novel structure for the victim’s GAN model to maximally retain the classification features of the real images.
- We conduct extensive experiments on three real-world datasets to comprehensively evaluate the performance of Anti-GAN. The results validate the efficacy of our scheme in protecting private images against GAN-based inference attacks.

2 PRELIMINARY

In this section, we introduce the general concepts of federated learning and generative adversarial networks.

2.1 Federated Learning

Federated learning (FL) [34] was initially proposed as a solution to the challenges of data isolation and data privacy protection. It facilitates collaborative training of a shared global model by multiple data holders, referred to as participants or clients, through a multi-round communication process. The FL workflow entails several key steps. First, all clients agree upon a specific structure for the global model. Subsequently, the server randomly selects a subset of clients and distributes the current state of the global model to each selected client. Finally, each selected client independently trains the model using their local data and exchanges model gradients with other clients through the server. Suppose N data holders $\{\mathcal{F}_1, \dots, \mathcal{F}_N\}$ wish to train a shared model \mathcal{M}_{FED} using their respective datasets $\{\mathcal{D}_1, \dots, \mathcal{D}_N\}$. The objective of federated learning can be formulated as $\min_{\theta} L(\theta)$ where $L(\theta) = \sum_{k=1}^N \frac{n_k}{n} \ell_k(\theta)$. $n_k = |\mathcal{D}_k|$ is the size of \mathcal{F}_k ’s dataset, $n = \sum_{k=1}^N n_k$ is the total number of training samples, and $\ell_k(\theta) = \frac{1}{n_k} \sum_{i \in \mathcal{D}_k} \ell(x_i, y_i; \theta)$ is the loss of \mathcal{F}_k ’s local model. $\ell(x_i, y_i; \theta)$ denotes the loss of prediction on sample point (x_i, y_i) with parameters θ .

2.2 Generative Adversarial Network

Generative Adversarial Network (GAN) [13] was initially developed for learning the distribution of training datasets. A GAN model consists of a generator G and a discriminator D . The goal of G is to produce synthetic samples $G(z)$ from random noise z in such a way that $G(z)$ are indistinguishable from real samples x according to the discriminator D . Typically, D and G engage in a minimax two-player game such that $\min_G \max_D V(D, G) = \mathbb{E}_{x \sim p_{data}(x)} [\log D(x)] + \mathbb{E}_{z \sim p_z(z)} [\log(1 - D(G(z)))]$, where p_{data} denotes the original data distribution, and p_z denotes the distribution of the noise variable z . $D(x)$ is the probability output by D that x originates from the real training data rather than being generated by the generator. Note that the traditional GANs, like DCGAN [41] and WGAN [14], cannot label the generated images and are thus unsuitable for our context, because the fake images generated by the victim’s GAN need to include both the inputs and labels for classification tasks. Instead, we employ Conditional GAN (CGAN) [37] to simultaneously generate images and labels. By feeding real labels y into both G and D , CGAN enables control over the classes of the generated images:

$$\min_G \max_D V_C(D, G) = \mathbb{E}_{x \sim p_{data}(x)} [\log D(x|y)] + \mathbb{E}_{z \sim p_z(z)} [\log(1 - D(G(z|y)))] \quad (1)$$

3 PROBLEM STATEMENT

Threat Model. There are two main threat models in GAN-based attacks: one or multiple participants are adversaries (e.g., [17]), and the central server is the adversary (e.g., [54]). Nevertheless, the basic ideas under these attacks are similar, i.e., the attacker leverages the shared model gradients as a discriminator and trains a generator to reconstruct the victim’s private data distribution. Without loss of generality, we focus on the *active* attack model in [17], where a single participant assumes the role of the attacker and can deviate from the training protocol to steal target information. Note that compared to the traditional semi-honest model [31], the active model provides significantly more benefits to the attacker and therefore presents greater challenges for mitigation.

Attacking Process. A typical attack scenario used in [17] is summarized as follows. Assume that participant A is the adversary and possesses data with labels $\{b, c\}$, while the victim participant V possesses data with labels $\{a, b\}$. The goal of participant A is to reconstruct the training data distribution belonging to class a owned by V . Note that the label heterogeneity among different participants plays a vital role in motivating GAN-based attacks [17, 54]. If the adversaries possess samples of the target class in their local datasets, there is no incentive for them to infer the representations of that specific target class. The attacking process unfolds as follows. First, V trains a local model honestly and uploads the model gradients to the central server. Next, A downloads these shared gradients and utilizes them to update the discriminator of the attack GAN model. Subsequently, A generates a data point with the label a using the GAN and falsely labels it as class c . A proceeds to train the local model using these pseudo-samples and shares the model parameters with V , aiming to entice the victim to provide more information about the class a . Ultimately, A can reconstruct an image of class a that is virtually indistinguishable from the samples in participant V ’s original images. In this paper, we aim to develop a defense method that can effectively prevent A from reconstructing plausible images from V ’s shared gradients.

It is worth noting that, unlike traditional FL scenarios [34], where participants receive only aggregated global gradients, the two-client scenario used in [17] allows the attacker to directly receive the victim’s gradients. This direct access poses substantial challenges for designing defense methods because, compared to traditional FL scenarios where gradient aggregation can balance out the private information contained in the victim’s gradients [55], the two-client scenario directly exposes the possible private information to attackers. Correspondingly, if our method can effectively

mitigate information leakage in the stringent two-client scenario, it can also be adopted in traditional FL scenarios, achieving equal or superior defense effects.

4 ANTI-GAN

In this section, we introduce the proposed defense mechanism, Anti-GAN, for mitigating the data leakage risks posed by GAN-based inference attacks. Note that the victim V is also referred to as the *defender* in this paper, as they are responsible for implementing the defense method.

The main idea of Anti-GAN is to obfuscate the visual features of private training images X that are used in the federated classifier. One approach is to train a CGAN model using X and generate a corresponding shadow image set X' with visually indistinguishable features. This shadow set X' is then utilized for the federated training process. However, this straightforward approach encounters two challenges. The first is how to corrupt the visual features of the generated image X' . The second is that this method may result in a degradation of accuracy in the federated model, because modifying the visual features of X simultaneously alters its distribution, leading to a potential mismatch between the distributions of the training dataset X' and the original (test) dataset X . To tackle these challenges, we design a three-step approach for Anti-GAN, i.e., obfuscating visual features, preserving classification features, and utilizing Mixup, to generate the final shadow images with desirable properties. In following subsections, we provide detailed explanations of each step.

4.1 Obfuscating Visual Features

Since the generated samples X' are utilized as the training dataset, the adversary retains the capability to reconstruct representative images of X' using the attack described in [17]. Therefore, in order to reduce the distinguishability of the reconstructed images, we need to obfuscate the visual features of X' before initiating the training process.

Note that GAN models are inclined to produce images with sharp details [21]. Inspired by PatchShuffle [47], we discovered that applying window-wise transformations to an image x can effectively obfuscate its local visual features (e.g., edges and corners) while preserving the overall features (e.g., image patterns). As a result, we design an unsupervised learning task for the defender's generator G to obfuscate the window-wise visual features of the generated images X' . Specifically, for each image x' (i.e., $G(z|y)$) generated by G , we divide it into m windows of size $s \times s$ and compute the following loss function:

$$\min_G \mathcal{L}_{\text{obf}} \quad \text{where} \quad \mathcal{L}_{\text{obf}} = \sum_{i=1}^m (Var(\mathbf{w}_i(G(z|y))) - v_e)^2, \quad (2)$$

where $Var(\mathbf{w}_i)$ denotes the pixel variance of window $\mathbf{w}_i \subseteq G(z|y)$; v_e is the *expected variance*, regulating the level of obfuscation for each window.

To demonstrate the effects of \mathcal{L}_{obf} , we employ the gradient descending method to modify the pixel values of an image according to Eq. (2) w.r.t. different v_e . The results are illustrated in Fig. 2a. By setting a variance threshold v_e close to the real image variance (e.g., 0.5), the defender can preserve the features of patches containing salient structures, while introducing significant noise to the flat patches, such as the background. Alternatively, by utilizing a larger v_e (e.g., 0.8), increased noise is introduced to obfuscate the entire image, while the overall features are still preserved.

4.2 Preserving Classification Features

GAN is used to learn the distribution of the training dataset X via an adversarial process [13]. However, the loss function \mathcal{L}_{obf} in Eq. (2) may hinder the learning process of GAN since it encourages the generator to produce images X' with a different pixel variance v_e than that of X .

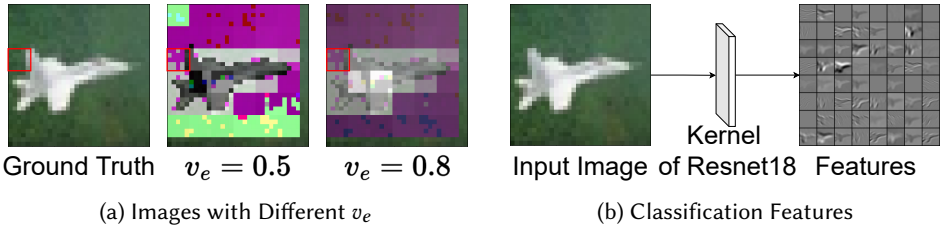


Fig. 2. (a) examples generated from Eq. (2), where the red box denotes a 5×5 window; (b) features extracted by the first convolutional layer of ResNet-18.

This difference can cause a decrease in the accuracy of the federated model tested on X as the distribution of X' may not match that of X . To address this issue, we propose to modify the GAN learning process such that the generated X' have similar classification features to those of X .

In the FL training phase, an image x' generated by GAN will be fed into the federated classifier, then this classifier determines the class of x' based on the classification features extracted by a series of convolutional and pooling layers. In other words, to reduce the performance degradation of the federated model after replacing the input X with X' , we only need to guarantee that the GAN correctly learns the distribution of the classification features of X , instead of the distribution of its visual features. Notice that in a deep neural network, the image features extracted by a higher layer (e.g., the final dense layer) are more specific to the task types, whereas the features extracted by a lower layer (e.g., the first convolutional layer) are more general for different tasks [62]. Inspired by this observation, we propose to use the first convolutional layer of ResNet-18 [16] pre-trained on ImageNet [8] as a *feature extractor* C to extract the low-level image features of x , as shown in Fig. 2b. The intuition for the choice of this feature extractor ¹ is that the ResNet-18 pre-trained on ImageNet is widely used in transfer learning, and its lower convolutional layers can extract extensive features and are general enough for different classification tasks.

After extracting the classification features $C(x)$ of x , we modify the objective function of the defender's GAN as:

$$\min_G \max_D \mathcal{L}_{\text{CGAN}} = \mathbb{E}_{x \sim p_{\text{data}}(x)} [\log D(C(x)|y)] + \mathbb{E}_{z \sim p_z(z)} [\log (1 - D(C(G(z)|y)))] \quad (3)$$

where $C(x)$ denotes the features of x extracted by C . The discriminator's task is now to distinguish between $C(X)$ and $C(X')$ instead of X and X' . In this way, we can ensure that X' has similar classification features to X , reducing the performance degradation of the federated model when X is replaced with X' . Finally, the objective function of the defender's GAN is given by

$$G^*(z^*) = \arg \min_G \max_D \mathcal{L}_{\text{CGAN}} + \min_G \lambda \mathcal{L}_{\text{obf}} \quad (4)$$

where λ is a hyperparameter controlling the effect of \mathcal{L}_{obf} . The structure of the revised GAN model is shown in Fig. 3.

4.3 Mixup

After training a CGAN model based on Eq. (4), X' can be generated and used as the training images of the federated model by the defender. However, our experiments show that the federated model f trained on X' suffers an accuracy degradation of approximately 20% when tested on X .

¹In the ablation study of Section 5.7, we replace the first convolutional layer of ResNet-18 with that of DesNet-121 [19] as the feature extractor C to evaluate the impact of different choices of C on the defense performance of Anti-GAN. The results demonstrate that the convolutional layers of both ResNet and DenseNet are effective within the framework of Anti-GAN.

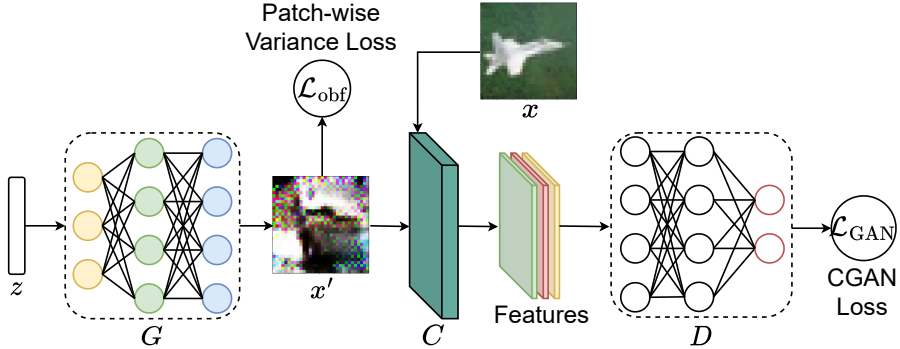


Fig. 3. The structure of the defender’s GAN.

compared to the model directly trained on X . The reason is that the feature extractor C of ResNet-18 has parameters that differ slightly from the parameters of the first convolutional layer C_f of f . The objective function $\mathcal{L}_{\text{CGAN}}$ can only guarantee that $C(x) \approx C(x')$ instead of $C_f(x) \approx C_f(x')$. This inconsistency between $C_f(x)$ and $C_f(x')$ can lead to the degradation of model accuracy. To further improve the performance of the federated model trained on X' , we use *Mixup* to combine the distributions of X and X' .

Mixup [65] is a data augmentation method used to enhance the generalization performance of classification models. In Mixup, a training image \hat{x} is generated by mixing two randomly selected private images: $\hat{x} = \mu x_1 + (1 - \mu)x_2$, where μ is a random number sampled from $[0, 1]$. The label \hat{y} is generated accordingly by $\hat{y} = \mu y_1 + (1 - \mu)y_2$, where y_1 and y_2 are one-hot labels. Considering that the one-hot label \hat{y} can leak the mixup parameter μ [20, 32], we employ a revised scheme in Anti-GAN to enhance the security of Mixup. For a specific class c , we first randomly sample a real image x with label c from X and then generate a fake image x' with label c from the defender’s CGAN. After that, the final training image \hat{x} is generated by $\hat{x} = \mu x + (1 - \mu)x'$, where μ is a tunable hyperparameter. The label \hat{y} of \hat{x} is naturally c and leaks no information of μ . Correspondingly, the defender’s final dataset \hat{X} for FL training is composed of a large number of \hat{x} . Note that to defend against the state-of-the-art attacks on Mixup [20, 32], we mix each real image x only once, which can effectively mitigate the possible risks [32]. Furthermore, it is worth noting that we combine two images into one training image, as mixing three or more images could lead to model performance degradation and increased computational costs during model training [65].

To conclude, we summarize the main steps of Anti-GAN in Algorithm 1 for reference.

Training Methods. As a game-theoretic framework, the training of Generative Adversarial Networks (GAN) is challenging due to the inherent instability of the optimization process [13]. Without careful parameter tuning, the generator of GAN may fail to converge to a stable point and generate meaningless outputs [41]. In Anti-GAN, in addition to the difficulty of GAN training, the hyperparameters including v_e in $\mathcal{L}_{\text{lobf}}$, the λ in the objective function (Eq. (4)), and the mixup parameter μ can all impact the quality of the training dataset \hat{X} . To achieve the desired quality of \hat{X} , we propose a two-step training method for Anti-GAN. First, we employ the objective function $\mathcal{L}_{\text{CGAN}}$ and the widely adopted training techniques² to train a CGAN until convergence. Then, we fine-tune the pre-trained CGAN by optimizing Eq. (4) and conduct a grid search to determine the optimal values of the hyperparameters $\{v_e, \lambda, \mu\}$. Our experimental trials demonstrate that this two-step method is more efficient than directly optimizing Eq. (4) from the beginning.

²<https://github.com/soumith/ganhacks>

Algorithm 1: The overview of Anti-GAN

Input: the private training dataset (X, Y) , the expected pixel variance v_e , the feature extractor C , the mixup parameter μ , the hyperparameter λ , a learning rate α

Output: The generated training dataset (\hat{X}, \hat{Y})

1 $\theta_G, \theta_D \leftarrow \mathcal{N}(0, 1)$; $\text{// Initialize the generator and discriminator}$

2 **while** θ_G and θ_D have not converged **do**

3 **for** each batch **do**

4 $\left\{ (x^{(i)}, y^{(i)}) \right\}_{i=1}^b \leftarrow$ randomly select a batch of samples ;

5 $\left\{ z^{(i)} \right\}_{i=1}^b \leftarrow$ sample a batch of random vectors ;

6 **for** $i \in \{1, \dots, b\}$ **do**

7 $\left(x^{(i)} \right)' \leftarrow G \left(z^{(i)}, y^{(i)}; \theta_G \right)$;

8 $\left\{ w_j^{(i)} \right\}_{j=1}^m \leftarrow$ divide $\left(x^{(i)} \right)'$ into m windows ;

9 $\ell_{\text{obf}} \leftarrow \frac{1}{b} \sum_{i=1}^b \mathcal{L}_{\text{obf}} \left(\left\{ w_j^{(i)} \right\}_{j=1}^m; v_e \right)$; $\text{// Obfuscate visual features}$

10 $\ell_{\text{CGAN}} \leftarrow \frac{1}{b} \sum_{i=1}^b \mathcal{L}_{\text{CGAN}} \left(C \left(x^{(i)} \right), C \left(\left(x^{(i)} \right)' \right), y^{(i)}; \theta_G, \theta_D \right)$;

11 $\ell_G \leftarrow \ell_{\text{CGAN}} + \lambda \ell_{\text{obf}}$

12 $\theta_G \leftarrow \theta_G - \alpha \cdot \nabla_{\theta_G} \ell_G$; $\text{// Update the generator}$

13 $\theta_D \leftarrow \theta_D - \alpha \cdot \nabla_{\theta_D} \ell_G$; $\text{// Update the discriminator}$

14 $(\hat{X}, \hat{Y}) \leftarrow \emptyset$;

15 **for** $i \in \{1, \dots, |X|\}$ **do**

16 $z^{(i)} \leftarrow$ sample a random vector ;

17 $\left(x^{(i)} \right)' \leftarrow G \left(z^{(i)}, y^{(i)}; \theta_G \right)$;

18 $\hat{x}^{(i)} \leftarrow \mu x^{(i)} + (1 - \mu) \left(x^{(i)} \right)'$; // Mixup

19 $(\hat{X}, \hat{Y}) \leftarrow (\hat{X}, \hat{Y}) \cup \left(\hat{x}^{(i)}, y^{(i)} \right)$;

20 **return** (\hat{X}, \hat{Y}) ;

5 EXPERIMENTS

In this section, we evaluate Anti-GAN *w.r.t.* the model performance degradation, as well as the defense effectiveness against GAN-based attacks. We begin by introducing the experimental setting. Following this, we present the defense performance of Anti-GAN under different parameter settings and compare its performance with DP-based defense methods.

5.1 Experimental Setting

Datasets. We evaluate the performance of Anti-GAN by conducting experiments on four image datasets: MNIST [61], FashionMNIST [59], CelebA [29], and CIFAR10 [27]. To ensure fair comparisons, we preprocess all images in these datasets by resizing them to 32×32 pixels and normalizing the pixel values to the range of $[-1, 1]$. In addition, we consider the CelebA dataset for a binary face recognition task, specifically, distinguishing between male and female faces.

Data Splitting. Regarding data splitting, we initially separate the images into two equal halves based on their classes. One half is allocated to the defender, and the other half is assigned to the attacker, following the approach outlined in [17]. It is important to note that this two-client FL

setup provides a notable advantage to the attacker due to the direct exposure of the gradients from the other participant. As a defense mechanism, if Anti-GAN demonstrates effectiveness within this two-client scenario, it inherently implies its viability within more conventional FL setups involving tens or hundreds of participants, because the private information contained in the defender’s gradients are naturally balanced out by the gradients contributed by other participants [55], thus significantly reducing the information available for recovery by the attacker, compared to the two-client setting.

Baseline. As discussed in Section 3, GAN-based attacks can be classified into client-side attack [17] and server-side attack [54]. Given the similarity in attack techniques employed by these two types of attacks, the resulting attack outcomes in our experiments are also similar across different settings. Therefore, for clarity, we present only the attack results generated by [17]. To the best of our knowledge, there is a lack of research dedicated to developing defenses against GAN-based attacks [17, 54] in the context of FL. Most privacy-preserving mechanisms [11, 43] in FL have been designed to combat gradient-based record-level attacks, making them unsuitable for addressing the challenges posed by GAN-based attacks. Nevertheless, to showcase the effectiveness of Anti-GAN, we compare its performance with DP-based FL frameworks [45, 49], in which the fundamental privacy-preserving building block is the DP-SGD [1] algorithm, a widely recognized privacy-preserving mechanism with robust theoretical guarantees. Specifically, in DP-SGD, to achieve (ϵ, δ) -differential privacy, the defender needs to inject random noises following specific distributions to the model gradients during each training epoch [1]. In addition, we compare Anti-GAN with a Dropout-based defense method [44], which was designed to counteract gradient-matching attacks [69] by regularizing the model to prevent it from memorizing private training data. Through a comparative analysis of accuracy degradation and defensive efficacy among Anti-GAN, the DP-based FL framework [45], and the Dropout-based defense method [44], we aim to provide insights into the superior privacy-utility trade-off of our proposed approach.

Implementation. We now introduce the implementation details of the attack algorithms and FL models in our experiments. The feature extractor utilized in Anti-GAN is the first convolutional layer of the ResNet-18³ pre-trained on ImageNet. All neural networks are implemented using the PyTorch⁴ framework and trained via the Adam optimizer [26] with a learning rate of 10^{-4} . DP mechanisms are implemented via the Opacus library [63]. All experiments are performed on a platform with NVIDIA GTX2060 GPU and AMD R7 4800H CPU. We employ CGAN as both the defender’s and the attacker’s GAN models in our study. Detailed structures of the GAN models and the federated classifier are provided in the Appendix for reference. During the experiments, we observed that variations in the window size specified in Eq. (2) and the parameter λ in Eq. (4) have negligible impact on the quality of the generated images in Anti-GAN. Therefore, for simplicity, we empirically set the window size to 4×4 and λ to 250 for all experiments. To eliminate potential outliers, we first conduct each experiment ten times independently and then report the averaged results in this paper.

Metrics. In our evaluation, we focus on two key aspects of Anti-GAN: the accuracy degradation of the federated model and its defensive performance against GAN-based attacks. To assess the *accuracy degradation* caused by Anti-GAN, we compute the Accuracy Degradation Ratio (ADR) by $ADR = \frac{a_{\hat{X}} - a_X}{a_X}$, where $a_{\hat{X}}$ denotes the accuracy of the federated model trained on \hat{X} generated by Anti-GAN and tested on the original images X , and a_X denotes the accuracy of the model trained and tested on X . Note that a smaller ADR indicates a lower level of accuracy degradation and better performance of Anti-GAN, and an ADR below 5% is considered acceptable in real-world

³https://pytorch.org/hub/pytorch_vision_resnet/

⁴<https://pytorch.org/>

applications [1, 20]. To evaluate the *defensive performance* of Anti-GAN against GAN-base attacks, we use \hat{X} to train the federated model f and then reconstruct X from f via the attack in [17]. The reconstructed images are denoted by \tilde{X} . After that, we compare the similarity between \tilde{X} and X via the mean Structural SIMilarity (SSIM) Index with a window size of 8×8 [52], which accounts for image luminance, contrast, and structure simultaneously. It is important to note that the commonly used ℓ_1 and ℓ_2 losses are not applicable in our case. Because these losses serve as record-level similarity metrics, focusing on pixel-level differences between individual images, rather than providing a comprehensive evaluation of group-level similarities.

Since the images in \tilde{X} are generated based on the distribution of \hat{X} and may not perfectly align with the images in X , we calculate $\text{SSIM}(\tilde{X}, X)$ as follows. First, we generate a set \tilde{X} containing 10,000 labeled images using the attacker’s GAN. For each labeled image $(\tilde{x}_i, \tilde{y}_i) \in \tilde{X}$, we compute the average $\text{SSIM}(\tilde{x}_i, x_j)$ between \tilde{x}_i and all images $x_j \in X$ with label $y_j = \tilde{y}_i$. Finally, we calculate $\text{SSIM}(\tilde{X}, X)$ by averaging the SSIM values across all $\tilde{x}_i \in \tilde{X}$:

$$\text{SSIM}(\tilde{X}, X) = \frac{1}{|\tilde{X}|} \sum_{\tilde{x}_i \in \tilde{X}} \frac{1}{|\{x_j\}|} \sum_{x_j \in X, y_j = \tilde{y}_i} \text{SSIM}(\tilde{x}_i, x_j). \quad (5)$$

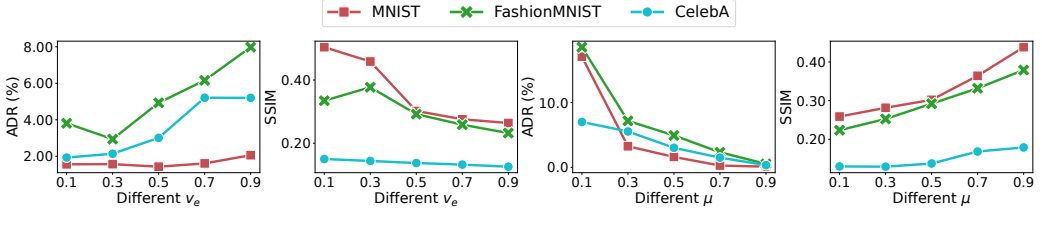
The resulting $\text{SSIM}(\tilde{X}, X)$ ranges from 0 to 1, where a higher SSIM indicates better visual features in \tilde{X} . Empirically, the generated images \tilde{X} are indistinguishable to human eyes if $\text{SSIM}(\tilde{X}, X) < 0.3$ [32].

5.2 Impact of Different Parameter Settings

The Expected Pixel Variance v_e . We firstly investigate the impact of different values of v_e on the performance of Anti-GAN. Recall that v_e represents the expected pixel variance of the generated images X' and controls the level of visual feature obfuscation in \mathcal{L}_{obf} (Eq. (2)). To evaluate the effect of varying v_e , we fix the Mixup parameter $\mu = 0.5$ and generate different training datasets \hat{X} with v_e values of 0.1, 0.3, 0.5, 0.7, and 0.9. We then assess the corresponding model ADR for the defender and the reconstruction performance for the attacker. Fig. 4a and 4b show the ADRs and SSIMs tested on Anti-GAN with different v_e values, respectively. Additionally, we provide visual examples of images generated by Anti-GAN as well as the attacker’s GAN in Figure 5a.

The depicted results allow for two key observations. *First*, the increase in v_e leads to a larger degradation in model accuracy, as depicted in Figure 4a. This outcome arises because higher values of v_e drive the distribution of X' further away from the distribution of X . Given that the original pixel variance of X is approximately 0.2, such a deviation could significantly alter the distribution of the training images, resulting in reduced testing accuracy of the model. *Second*, the rise in v_e introduces more noise into the training images \hat{X} , thereby diminishing the distinguishability of the images generated by the attacker’s GAN, as evident in Figure 4b and 5a. The presence of additional noise obscures the details of the original images X , making them less recoverable by the GAN. Notably, GAN-based reconstruction yields poor visual quality in the restored images \tilde{X} when $v_e \geq 0.5$, rendering it challenging to discern the edges and corners in MNIST and the facial features in CelebA. Therefore, a privacy-utility trade-off is evident in Anti-GAN as v_e increases. Notably, when $v_e \leq 0.5$, the ADRs on the tested datasets remain below 5%, while the SSIM values achieved by the attacker generally fall below 0.3 when $v_e \geq 0.5$. This observation suggests that a v_e value of 0.5 strikes the optimal privacy-utility balance.

The Mixup Parameters μ . In this section, we assess the impact of the parameter μ on the performance of Anti-GAN, where μ controls the amount of information from the real images X incorporated into the training images \hat{X} . To evaluate the effect of μ , we fix v_e at 0.5 and generate different training datasets \hat{X} by varying μ across the values of 0.1, 0.3, 0.5, 0.7, and 0.9. We then



(a) Accuracy Degradation (b) Attack Performance (c) Accuracy Degradation (d) Attack Performance

Fig. 4. (a)-(b): The accuracy degradation of the federated model and the performance of GAN-based attacks under Anti-GAN with different pixel variances v_e and $\mu = 0.5$; (c)-(d): the accuracy degradation and attack performance tested under Anti-GAN with different mixup parameters μ and $v_e = 0.5$.

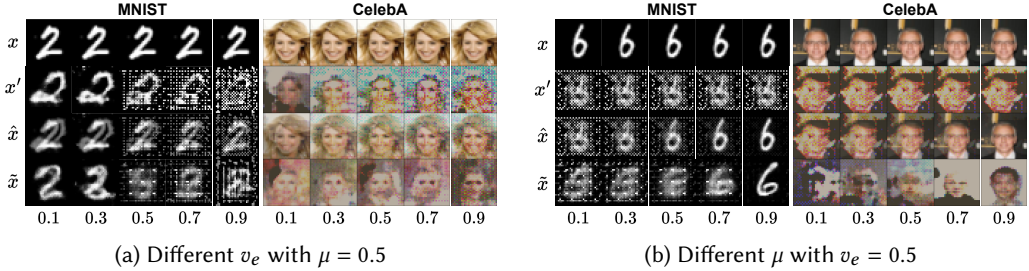


Fig. 5. Examples generated with different (a) pixel variance v_e and (b) Mixup parameter μ . x denotes the original images, x' denotes the images generated by the defender's GAN, \hat{x} denotes the Mixup images of x and x' , and \tilde{x} denotes the restored images by [17]. Note that the images of \tilde{x} do not correspond to \hat{x} in a one-to-one manner, as GAN models are capable of generating only class representations rather than the original training images.

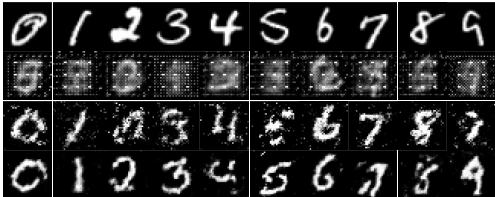
analyze the ADRs of the federated model and the SSIMs achieved by the attacker, as depicted in Figure 4c and 4d, respectively. Additionally, Figure 5b showcases visual examples of images generated with different μ values. Our observations reveal the existence of a privacy-utility trade-off with respect to μ . Generally, increasing μ can reduce the degradation in the accuracy of the federated model, as shown in Figure 4c. This outcome stems from the fact that higher μ values result in a larger portion of the real images X being incorporated into the training images \hat{X} . Consequently, the distribution of \hat{X} becomes closer to the distribution of X , leading to improved testing performance. However, the increase in μ also provides more advantages to the attacker's GAN model, as demonstrated in Figure 4d. A larger μ implies that clearer visual features of X are present in \hat{X} , making it easier for the attacker to restore more accurate images and increasing the risk of information leakage. Moreover, $\mu = 0.5$ achieves the best privacy-utility trade-off, as it prevents the attacker from generating distinguishable images ($SSIM < 0.3$) while causing minimal harm to model accuracy ($ADR < 5\%$).

5.3 Comparison with Related Defense Mechanisms

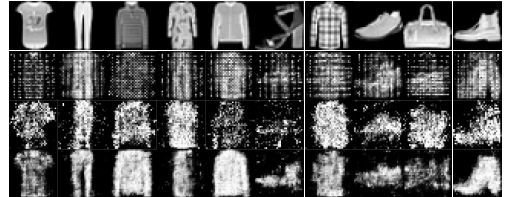
In this section, we compare Anti-GAN with the DP-based FL framework [45] and the Dropout-based method [44] in preserving privacy while maintaining model utility. For Anti-GAN, we follow the parameter settings suggested in Section 5.2, namely $\mu = 0.5$ and $v_e = 0.5$. As for DP, we adopt a fixed privacy budget of $\delta = 10^{-5}$ as suggested in [1] and vary the privacy budget ϵ across

Table 1. Performance comparison between Anti-GAN ($v_e = 0.5$, $\mu = 0.5$), DP-based FL framework [45], and Dropout-based method [44].

Methods	Parameters	ADR				SSIM			
		MNIST	F.MNIST	CelebA	CIFAR10	MNIST	F.MNIST	CelebA	CIFAR10
Anti-GAN	/	1.61%	4.93%	3.02%	8.84%	0.3020	0.2920	0.1372	0.0933
DP-based [45]	$\epsilon = 0.5$	6.20%	11.94%	7.69%	41.01%	0.4515	0.2921	0.1851	0.1122
	$\epsilon = 1$	5.42%	10.22%	6.33%	34.58%	0.4893	0.3175	0.2168	0.1219
	$\epsilon = 2$	4.94%	8.99%	3.46%	30.38%	0.5006	0.3491	0.2960	0.1472
	$\epsilon = 4$	3.62%	7.96%	2.92%	28.04%	0.5303	0.3552	0.3245	0.1598
	$\epsilon = 8$	2.32%	7.39%	2.45%	20.73%	0.5365	0.3853	0.3664	0.1540
Dropout-based [44]	$p = 0.1$	-0.12%	-0.09%	-0.01%	1.24%	0.5627	0.3962	0.3602	0.1575
	$p = 0.5$	-0.18%	1.67%	1.51%	3.01%	0.5544	0.4048	0.3796	0.1634



(a) MNIST



(b) FashionMNIST

Fig. 6. The image examples reconstructed by the adversary’s GAN model. The first row denotes the original private images, the second row denotes the images reconstructed from Anti-GAN, the third row denotes the images reconstructed from DP FL with $\epsilon = 0.5$, and the fourth row denotes the images reconstructed from DP FL with $\epsilon = 8$.

the values of $\{0.5, 1, 2, 4, 8\}$ to train different local models based on X . These privacy-preserving models are then utilized as the discriminator in the attacker’s GAN to learn the distribution of X . For the Dropout-based method, we follow the parameter setting in [44] and set the dropout rates $p \in \{0.1, 0.5\}$ after each layer of the testing models. Table 1 presents the ADRs and SSIMs obtained from Anti-GAN, the DP-based method [45], and the Dropout-based method [44]. Furthermore, Figure 6 showcases example images reconstructed using Anti-GAN (the second row), DP FL with $\epsilon = 0.5$ (the third row), and DP FL with $\epsilon = 8$ (the fourth row). From these results, we draw three main observations. First, as shown in Table 1, Anti-GAN incurs the least accuracy degradation in the MNIST, FashionMNIST, and CIFAR10 datasets compared to the DP-based method [45], while achieving superior defensive performance across all the testing datasets. Second, while setting $\epsilon = 0.5$ in DP FL can provide some mitigation against GAN-based attacks, as depicted in Figure 6b, the defensive performance of DP FL is limited for simple image patterns, such as digital numbers in Figure 6a. Additionally, smaller ϵ values (< 4) may lead to accuracy degradation exceeding 5%, which could be deemed unacceptable for business companies [2]. Third, the Dropout-based method [44] incurs minimal accuracy degradation and, under certain conditions, even enhances model performance. This is anticipated as the method in [44] can act as a regularization approach that can improve the model’s generalization performance. However, its defensive efficacy, as reflected in the SSIM scores for image reconstruction, is the lowest among the three methods. This suggests that the Dropout-based method is less effective in preventing the memorization of training image distributions, thereby offering limited protection against GAN-based attacks [17]. In



Fig. 7. The images reconstructed by the gradient matching attack [69] without (the second row) and with (the third row) Anti-GAN. The first row shows the ground truth images.

summary, Anti-GAN achieves a more favorable privacy-utility trade-off compared to the DP-based method [45] and the Dropout-based method [44].

5.4 Defense Performance against Record-Level Attacks

Given that Anti-GAN is specifically designed to prevent GAN-based attacks [17, 54] from retrieving group-level information, an intriguing question arises: can Anti-GAN effectively counteract attacks at the individual record level? In this section, we evaluate Anti-GAN’s defense performance against the gradient-matching attacks [69], which aims to reconstruct individual training images via the shared model gradients.

Fig. 7 shows examples reconstructed by the gradient-matching method proposed in [69], both without and with the safeguard of Anti-GAN. The images in the second row indicate that gradient-matching attacks can accurately reconstruct original training images at the pixel level. Contrarily, the visual features of the reconstructed images in the third row are obscured, rendering details such as hair and glasses indistinguishable in human faces. This observation demonstrates Anti-GAN’s capability to substantially degrade the performance of record-level gradient-matching attacks in federated learning. The rationale behind this lies in Anti-GAN’s inherent ability to obfuscate visual features in input images. Consequently, while gradient-matching attacks can accurately reconstruct inputs pixel by pixel, the recovered images remain visually blurred.

The findings in Fig. 7 underscore that, beyond countering group-level attacks, Anti-GAN can effectively mitigate record-level attacks.

5.5 Evaluation of Privacy Leakage on Different Visual Features

In this section, we present experimental results on the CelebA dataset to evaluate whether an attacker can exploit low-quality images generated by Anti-GAN to infer various private visual features. Specifically, we investigate whether Anti-GAN, trained on the gender classification task, can protect the privacy of additional visual features such as hair color and eyeglasses. In the experiment, we first train classifiers on real images labeled with various visual attributes including black hair, eyeglasses, smiling, and young. These classifiers, once well-trained, are then utilized to predict the labels of images generated by Anti-GAN. We employ entropy to quantify the uncertainty of model predictions post-softmax [50]: $H(p) = -\sum_i p_i(x) \log p_i(x)$, where $p_i(x)$ denotes the probability of x being assigned label i in the model predictions, and higher $H(p)$ values indicate greater uncertainty in the model’s predictions. The entropy values of model predictions on Anti-GAN for the visual features {black hair, eyeglasses, smiling, young} are {0.5846, 0.5574, 0.6086, 0.631}, respectively. For comparison, the entropy values of model predictions on real images for the four visual features are {0.4167, 0.1929, 0.3426, 0.5211}, and the entropy of random guesses is 0.6931. These results demonstrate that Anti-GAN can substantially increase the uncertainty in model predictions on the generated images with obfuscated visual features, nearly

Table 2. Performance comparison under different client settings.

Client Settings	ADR			SSIM		
	MNIST	FashionMNIST	CelebA	MNIST	FashionMNIST	CelebA
2 Clients	1.61%	4.93%	3.02%	0.3020	0.2920	0.1372
4 Clients	1.19%	4.90%	3.09%	0.3053	0.2985	0.1329
8 Clients	1.08%	4.66%	3.22%	0.3042	0.2841	0.1387
16 Clients	0.98%	4.45%	2.89%	0.2478	0.2738	0.1252
32 Clients	0.81%	4.54%	2.16%	0.2345	0.2506	0.1203

to the level of random guesses, thus significantly mitigating the risks of privacy leakage for various visual features.

5.6 Defense Performance under Different Client Settings

In this section, we evaluate the performance of Anti-GAN under different client configurations within the FL framework. The numbers of clients are chosen from $\{2, 4, 8, 26, 32\}$. Note that GAN-based attacks [17] are effective only in scenarios where the adversary does not possess the target data distribution, which means that the data distribution among different clients in FL should be heterogeneous, non-iid distributions. In the experiment, we first randomly divide the training data into two halves based on class distribution and similarly partition the clients into two groups. Then, each client in the first group is assigned a specific number of data samples randomly chosen from the first half of the training set, while clients in the second group receive samples from the second half. This approach ensures that the data distributions between the two client groups differ significantly, thereby enabling the attacker in one group to infer the data distribution of a defender in the opposite group using GAN-based attacks. To more accurately reflect real-world FL scenarios, we progressively reduce the number of samples per client as the number of clients increases. Specifically, the sample sizes per client for client configurations $\{2, 4, 8, 26, 32\}$ are set to $\{6000, 4000, 2000, 1000, 500\}$, respectively.

Table 2 presents the performance of Anti-GAN across different client configurations. Notably, as the number of clients in the FL framework increases, the degradation in accuracy caused by Anti-GAN diminishes. This trend is due to the reduction in data samples per client as the number of clients rises, which leads to fewer generated samples being used by the defender during training, thereby mitigating the negative impact of Anti-GAN on the performance of the federated model. Furthermore, the data in Table 2 demonstrate that as the number of clients increases, the defense performance of Anti-GAN improves, reflected by a reduction in SSIM scores for image reconstruction. This improvement can be attributed to the limitations of GAN-based attacks [17], which depend on the gradients uploaded by the defender to train the adversarial generator. As the number of samples owned by the defender decreases, the useful information in the uploaded gradients diminishes, thereby hindering the adversary’s ability to generate plausible images. In summary, increasing the number of participating clients in the FL framework can enhance the performance of Anti-GAN.

5.7 Ablation Study

Anti-GAN comprises three key components: the loss function \mathcal{L}_{obf} for obfuscating the visual features of X' , the feature extractor for preserving the classification features of X in X' , and the Mixup step for enhancing the performance of the federated model. To assess the effectiveness of these components, we remove each component in turn and evaluate the performance of the

Table 3. Results of the ablation study.

Branch	The Original Anti-GAN	No \mathcal{L}_{obf}	No Feature Extractor C	No Mixup	DenseNet Extractor C
ADR	1.61%	0.96%	1.98%	22.55%	1.45%
SSIM	0.3020	0.5680	0.3467	0.2446	0.3037
x					
x'					
\hat{x}					
\tilde{x}					

modified Anti-GAN accordingly. The MNIST dataset is utilized for testing purposes in this study. It is important to note that the default parameter configuration of Anti-GAN is set to $\mu = 0.5$ and $v_e = 0.5$. Table 3 presents the ADR and SSIM metrics, along with sample images of X , X' , \hat{X} , and \tilde{X} corresponding to different branches of Anti-GAN, from which we make three observations.

First, the model trained without incorporating the \mathcal{L}_{obf} component within Anti-GAN exhibits the least accuracy degradation. However, the attacker is able to successfully restore the private images with the best visual features. This implies that this modified Anti-GAN provides minimal protection for the defender’s private images against GAN-based attacks. This outcome is expected, as the visual features of X' learned by the defender’s GAN model are roughly equivalent to those of X , thereby offering limited safeguarding for X .

Second, in the absence of a feature extractor component, the impact of \mathcal{L}_{obf} is somewhat neutralized by the learning process of the defender’s GAN model. Consequently, the visual features of the generated X' become closer to those of X , resulting in a superior attack performance compared to the original Anti-GAN. Concurrently, the defender’s GAN primarily focuses on learning the visual features rather than the classification features of X , leading to a more substantial degradation in accuracy.

Third, the model trained without the Mixup component experiences the most pronounced accuracy degradation, while the attacker struggles to extract useful information from the training images \hat{X} (i.e., X'). As discussed in Section 4.3, the distribution of X' learned by the defender’s GAN model can deviate significantly from that of X . By incorporating Mixup, which involves the mixing of X' with X , we can substantially enhance the model’s accuracy, as demonstrated in the original Anti-GAN branch of Table 3.

Furthermore, we evaluate the effectiveness of the ResNet feature extractor by substituting it with the first convolutional layer of a pre-trained DesNet-121 [19] and then perform experiments on the DesNet feature extractor. The results in Table 3 show that the defense performance of Anti-GAN on the DenseNet feature extractor is comparable to the performance on the ResNet extractor, indicating that the first convolutional layers of various pre-trained deep models can be effectively utilized within the Anti-GAN framework.

In summary, the ablation study shows that the original Anti-GAN achieves the optimal privacy-utility trade-off, thereby validating the effectiveness of different components in our design.

6 DISCUSSION

Unlike traditional inference attacks [31, 69] that focus on inferring privacy at the individual record level, the GAN-based attack [17] targets the recovery of group-level information (data distribution) in private datasets. While DP [1, 60] offers robust protection against record-level attacks, the development of defense mechanisms with theoretical guarantees against group-level attacks is still limited. One approach to protect group-level information is to extend traditional DP mechanisms to group-level settings, as described in [23, 66]. However, this approach may result in significant accuracy degradation for the model. For instance, training a federated classifier on Cifar-10 with a privacy budget of $\epsilon = 1.5$ can lead to up to 16.99% accuracy degradation [66]. The research on defense mechanisms that can simultaneously defend against group-level attacks while preserving model utility is still limited. Our work represents the first study to explore defense mechanisms for protecting group-level information while minimizing model performance degradation. The analysis of the theoretical privacy guarantee of Anti-GAN is challenging due to its objective of obfuscating the visual distribution of the training images \hat{X} . Because, unlike pixel values, there are currently no widely recognized metrics that can precisely quantify the visual indistinguishability between images restored by GAN-based attacks and the original images. Additionally, the level of indistinguishability of visual features is subjective and may vary among different human observers. Nevertheless, our study represents an initial step in the development of defense mechanisms for protecting group-level information. While Anti-GAN is an empirical study, our experimental results demonstrate its effectiveness in defending against GAN-based attacks compared to traditional DP mechanisms, with minimal impact on model accuracy, typically below 5%.

7 RELATED WORK

Inference Attacks on Machine Learning. Machine Learning (ML) algorithms are vulnerable to various forms of inference attacks, including membership inference [36, 40, 42, 46], property inference [10, 24, 33, 36, 53], and feature inference (also known as model inversion) [9, 17, 22, 30, 31, 54, 56, 69]. Membership inference attacks determine whether a specific sample is part of the training dataset. [46] introduces a shadow model training technique for membership inference, which is later improved by [42] under loose assumptions, and by [40] in the setting of federated learning. Property inference attacks aim to infer aggregate statistics of the training dataset, such as the statistics of software execution traces [10] and the age distribution of a bank’s customer data [24]. Feature inference attacks attempt to reconstruct the original inputs from ML applications. [9] explores model inversion attacks in decision trees and neural networks using labels and black-box access to the target model. [31] proposes to infer the training records in federated learning via model predictions. [69] restores the private training data using only model gradients. In federated learning, recent studies exploit feature inference attacks based on GANs. [17] proposes a GAN-based threat model where an adversary tries to extract representatives of a class not owned by him. By taking the shared global model as the discriminator of GAN, the adversary can further mislabel the pseudo-samples generated by the generator to trick other participants into leaking more private information. [54] assumes a malicious server and utilizes GANs to explore user-level privacy leakage, similar to the method in [17]. Note that in the literature, GANs have also been used in other types of attacks, such as membership inference attacks [7, 28], backdoor attacks [18, 35], and adversarial attacks [39, 70]. In this paper, we focus on *GAN-based feature inference attacks*. The main difference between GAN-based feature inference attacks [17, 54] and traditional feature inference attacks [9, 22, 31, 56, 69] is that the former focuses on inferring class representations (i.e., group-level information) via a GAN model from model gradients, whereas the latter aims to restore record-level private information (i.e., individual model inputs) from publicly released

information, such as data labels [9], model predictions [31], and gradients [69]. Record-level feature inference attacks can be effectively mitigated by state-of-the-art defense mechanisms in FL, such as dropout [36, 42], differential privacy [3, 45], and secure multiparty computation [4]. However, GAN-based feature inference attacks pose significant challenges for mitigation. The effectiveness of these attacks is closely tied to the practicality of the federated model [17], making them difficult to defend against. To the best of our knowledge, there are no defense mechanisms that can effectively counter GAN-based attacks without causing substantial performance degradation to the federated model. In this paper, we focus on developing defenses against GAN-based feature inference attacks [17, 54] that can achieve a favorable privacy-utility trade-off.

Defenses against Inference Attacks. Numerous defense methods have been proposed to mitigate the risks incurred by inference attacks, including dropout [36, 42, 44], model stacking [42], mutual information-based regularization [51], anomaly detection [3], differential privacy [3, 12, 15, 23, 45], secure multiparty computation [4, 38, 49, 57, 64], and InstaHide [20]. Dropout [36, 42, 44] and model stacking [42] are basically regularization methods, which are mainly used to prevent model overfitting, thereby reducing the amount of information memorized by ML models. Anomaly detection [3] is utilized to mitigate poisoning-based attacks performed by active adversaries. Traditional differential privacy methods [3, 15, 45] provide rigorous theoretical guarantees for privacy protection, but they are applicable to individual-level attacks instead of group-level attacks. Although recent studies [12, 23] have extended DP guarantees to group-level privacy, these methods can significantly degrade model performance. Secure multiparty computation [4, 38, 57] can impose substantial computational costs during model training and has not been widely applied in real-world applications. Among these defense methods, InstaHide [20] is most similar to our approach, i.e., using *Mixup* [65] to corrupt the visual features of private training images. However, there are three main differences between InstaHide and Anti-GAN. First, InstaHide mixes multiple real images into one training image, while our scheme uses a GAN model to generate multiple fake images and then mixes these fake images with real images. Second, InstaHide obfuscates image visual features by randomly flipping pixel signs, leading to uncontrollable model performance degradation. In contrast, Anti-GAN obfuscates visual features using a specifically designed loss function, allowing the privacy-utility tradeoff to be tuned for different application scenarios. Third, [5] and [32] have experimentally demonstrated that private images can be reconstructed from the mixup images generated by InstaHide on the condition that the same private image is mixed into multiple training images. Our scheme mitigates this risk by ensuring that each private image is mixed only once. It is important to note that none of the aforementioned defenses, including InstaHide, are specifically designed to counter GAN-based attacks. To the best of our knowledge, this is the *first* paper to exploit defenses against GAN-based feature inference attacks in the context of federated learning.

8 CONCLUSION

In this paper, we introduce Anti-GAN, a novel approach designed to protect the privacy of participants' training data against GAN-based feature inference attacks in the context of federated learning. By strategically distorting the original distribution of the private training dataset, Anti-GAN effectively prevents attackers from generating distinguishable images while maintaining a high-performance federated classifier. Our experimental results demonstrate that, compared to the widely adopted DP-SGD mechanism, which can degrade model accuracy by up to 12% and allow for a similarity score of up to 0.53 for image reconstruction, our method limits model accuracy degradation to a maximum of 5% and reduces the similarity scores of reconstructed images to at most 0.30. In addition, our experiments show that Anti-GAN can not only defend against GAN-based feature inference attacks but also provide protection against gradient-based record-level

reconstruction attacks. This study represents an initial step toward developing defense mechanisms against GAN-based attacks that can achieve a favorable privacy-utility tradeoff, and we believe it can contribute valuable insights into the advancement of privacy-preserving mechanisms in the context of federated learning.

REFERENCES

- [1] Martin Abadi, Andy Chu, Ian Goodfellow, H Brendan McMahan, Ilya Mironov, Kunal Talwar, and Li Zhang. 2016. Deep learning with differential privacy. In *Proceedings of the 2016 ACM SIGSAC conference on computer and communications security*. 308–318.
- [2] Apple.com. 2023. Differential Privacy. https://www.apple.com/privacy/docs/Differential_Privacy_Overview.pdf. Online; accessed 28-July-2024.
- [3] Eugene Bagdasaryan, Andreas Veit, Yiqing Hua, Deborah Estrin, and Vitaly Shmatikov. 2020. How to backdoor federated learning. In *International conference on artificial intelligence and statistics*. PMLR, 2938–2948.
- [4] Keith Bonawitz, Vladimir Ivanov, Ben Kreuter, Antonio Marcedone, H Brendan McMahan, Sarvar Patel, Daniel Ramage, Aaron Segal, and Karn Seth. 2017. Practical secure aggregation for privacy-preserving machine learning. In *Proceedings of the 2017 ACM SIGSAC Conference on Computer and Communications Security*. 1175–1191.
- [5] Nicholas Carlini, Samuel Deng, Sanjam Garg, Somesh Jha, Saeed Mahloujifar, Mohammad Mahmoodi, Abhradeep Thakurta, and Florian Tramèr. 2021. Is private learning possible with instance encoding?. In *2021 IEEE Symposium on Security and Privacy (SP)*. IEEE, 410–427.
- [6] Nicholas Carlini, Chang Liu, Úlfar Erlingsson, Jernej Kos, and Dawn Song. 2019. The secret sharer: Evaluating and testing unintended memorization in neural networks. In *28th USENIX security symposium (USENIX security 19)*. 267–284.
- [7] Dingfan Chen, Ning Yu, Yang Zhang, and Mario Fritz. 2020. Gan-leaks: A taxonomy of membership inference attacks against generative models. In *Proceedings of the 2020 ACM SIGSAC conference on computer and communications security*. 343–362.
- [8] Jia Deng, Wei Dong, Richard Socher, Li-Jia Li, Kai Li, and Li Fei-Fei. 2009. Imagenet: A large-scale hierarchical image database. In *2009 IEEE conference on computer vision and pattern recognition*. Ieee, 248–255.
- [9] Matt Fredrikson, Somesh Jha, and Thomas Ristenpart. 2015. Model inversion attacks that exploit confidence information and basic countermeasures. In *Proceedings of the 22nd ACM SIGSAC Conference on Computer and Communications Security*. 1322–1333.
- [10] Karan Ganju, Qi Wang, Wei Yang, Carl A Gunter, and Nikita Borisov. 2018. Property inference attacks on fully connected neural networks using permutation invariant representations. In *ACM CCS*. 619–633.
- [11] Wei Gao, Shangwei Guo, Tianwei Zhang, Han Qiu, Yonggang Wen, and Yang Liu. 2021. Privacy-Preserving Collaborative Learning With Automatic Transformation Search. In *IEEE Conference on Computer Vision and Pattern Recognition, CVPR 2021, virtual, June 19-25, 2021*. Computer Vision Foundation / IEEE, 114–123.
- [12] Robin C Geyer, Tassilo Klein, and Moin Nabi. 2017. Differentially private federated learning: A client level perspective. *arXiv preprint arXiv:1712.07557* (2017).
- [13] Ian Goodfellow, Jean Pouget-Abadie, Mehdi Mirza, Bing Xu, David Warde-Farley, Sherjil Ozair, Aaron Courville, and Yoshua Bengio. 2014. Generative adversarial nets. In *Advances in neural information processing systems*. 2672–2680.
- [14] Ishaan Gulrajani, Faruk Ahmed, Martin Arjovsky, Vincent Dumoulin, and Aaron C Courville. 2017. Improved training of wasserstein gans. In *Advances in neural information processing systems*. 5767–5777.
- [15] Chuan Guo, Brian Karrer, Kamalika Chaudhuri, and Laurens van der Maaten. 2022. Bounding training data reconstruction in private (deep) learning. In *International Conference on Machine Learning*. PMLR, 8056–8071.
- [16] Kaiming He, Xiangyu Zhang, Shaoqing Ren, and Jian Sun. 2016. Deep residual learning for image recognition. In *Proceedings of the IEEE conference on computer vision and pattern recognition*. 770–778.
- [17] Briland Hitaj, Giuseppe Ateniese, and Fernando Perez-Cruz. 2017. Deep models under the GAN: information leakage from collaborative deep learning. In *Proceedings of the 2017 ACM SIGSAC Conference on Computer and Communications Security*. 603–618.
- [18] Weiwei Hu and Ying Tan. 2022. Generating adversarial malware examples for black-box attacks based on GAN. In *International Conference on Data Mining and Big Data*. Springer, 409–423.
- [19] Gao Huang, Zhuang Liu, Laurens Van Der Maaten, and Kilian Q Weinberger. 2017. Densely connected convolutional networks. In *Proceedings of the IEEE conference on computer vision and pattern recognition*. 4700–4708.
- [20] Yangsibo Huang, Zhao Song, Kai Li, and Sanjeev Arora. 2020. Instahide: Instance-hiding schemes for private distributed learning. In *International Conference on Machine Learning*. PMLR, 4507–4518.
- [21] Phillip Isola, Jun-Yan Zhu, Tinghui Zhou, and Alexei A Efros. 2017. Image-to-image translation with conditional adversarial networks. In *Proceedings of the IEEE conference on computer vision and pattern recognition*. 1125–1134.

[22] Bargav Jayaraman and David Evans. 2022. Are attribute inference attacks just imputation?. In *Proceedings of the 2022 ACM SIGSAC Conference on Computer and Communications Security*. 1569–1582.

[23] Yangfan Jiang, Xinjian Luo, Yuncheng Wu, Xiaokui Xiao, and Beng Chin Ooi. 2024. Protecting Label Distribution in Cross-Silo Federated Learning. In *2024 IEEE Symposium on Security and Privacy (SP)*. IEEE Computer Society, 113–113.

[24] Yangfan Jiang, Xinjian Luo, Yuncheng Wu, Xiaochen Zhu, Xiaokui Xiao, and Beng Chin Ooi. 2024. On Data Distribution Leakage in Cross-Silo Federated Learning. *IEEE Trans. Knowl. Data Eng.* 36, 7 (2024), 3312–3328.

[25] Marcel Keller. 2020. MP-SPDZ: A versatile framework for multi-party computation. In *Proceedings of the 2020 ACM SIGSAC conference on computer and communications security*. 1575–1590.

[26] Diederik P. Kingma and Jimmy Ba. 2015. Adam: A Method for Stochastic Optimization. In *3rd International Conference on Learning Representations, ICLR 2015, San Diego, CA, USA, May 7-9, 2015, Conference Track Proceedings*.

[27] Alex Krizhevsky, Geoffrey Hinton, et al. 2009. Learning multiple layers of features from tiny images. (2009).

[28] Zinan Lin, Vyas Sekar, and Giulia Fanti. 2021. On the privacy properties of gan-generated samples. In *International Conference on Artificial Intelligence and Statistics*. PMLR, 1522–1530.

[29] Ziwei Liu, Ping Luo, Xiaogang Wang, and Xiaoou Tang. 2015. Deep Learning Face Attributes in the Wild. In *Proceedings of International Conference on Computer Vision (ICCV)*.

[30] Xinjian Luo, Yangfan Jiang, and Xiaokui Xiao. 2022. Feature Inference Attack on Shapley Values. In *Proceedings of the 2022 ACM SIGSAC Conference on Computer and Communications Security*. 2233–2247.

[31] Xinjian Luo, Yuncheng Wu, Xiaokui Xiao, and Beng Chin Ooi. 2021. Feature inference attack on model predictions in vertical federated learning. In *2021 IEEE 37th International Conference on Data Engineering (ICDE)*. IEEE, 181–192.

[32] Xinjian Luo, Xiaokui Xiao, Yuncheng Wu, Juncheng Liu, and Beng Chin Ooi. 2022. A Fusion-Denoising Attack on InstaHide with Data Augmentation. In *Proceedings of the AAAI Conference on Artificial Intelligence*, Vol. 36. 1899–1907.

[33] Saeed Mahloujifar, Esha Ghosh, and Melissa Chase. 2022. Property Inference from Poisoning. In *IEEE S&P*. IEEE, 1120–1137.

[34] Brendan McMahan, Eider Moore, Daniel Ramage, Seth Hampson, and Blaise Aguera y Arcas. 2017. Communication-efficient learning of deep networks from decentralized data. In *Artificial intelligence and statistics*. PMLR, 1273–1282.

[35] Haochen Mei, Gaolei Li, Jun Wu, and Longfei Zheng. 2023. Privacy inference-empowered stealthy backdoor attack on federated learning under non-iid scenarios. In *2023 International Joint Conference on Neural Networks (IJCNN)*. IEEE, 1–10.

[36] Luca Melis, Congzheng Song, Emiliano De Cristofaro, and Vitaly Shmatikov. 2019. Exploiting unintended feature leakage in collaborative learning. In *2019 IEEE Symposium on Security and Privacy (SP)*. IEEE, 691–706.

[37] Mehdi Mirza and Simon Osindero. 2014. Conditional generative adversarial nets. *arXiv preprint arXiv:1411.1784* (2014).

[38] Payman Mohassel and Yupeng Zhang. 2017. SecureML: A System for Scalable Privacy-Preserving Machine Learning. In *IEEE S&P*. 19–38.

[39] Dongbin Na, Sangwoo Ji, and Jong Kim. 2022. Unrestricted black-box adversarial attack using gan with limited queries. In *European Conference on Computer Vision*. Springer, 467–482.

[40] Milad Nasr, Reza Shokri, and Amir Houmansadr. 2019. Comprehensive privacy analysis of deep learning: Passive and active white-box inference attacks against centralized and federated learning. In *2019 IEEE symposium on security and privacy (SP)*. IEEE, 739–753.

[41] Alec Radford, Luke Metz, and Soumith Chintala. 2016. Unsupervised Representation Learning with Deep Convolutional Generative Adversarial Networks. In *4th International Conference on Learning Representations, ICLR 2016, San Juan, Puerto Rico, May 2-4, 2016, Conference Track Proceedings*.

[42] Ahmed Salem, Yang Zhang, Matthias Humbert, Pascal Berrang, Mario Fritz, and Michael Backes. 2019. ML-Leaks: Model and Data Independent Membership Inference Attacks and Defenses on Machine Learning Models. In *26th Annual Network and Distributed System Symposium, NDSS 2019, San Diego, California, USA, February 24-27, 2019*. The Internet Society.

[43] Daniel Scheliga, Patrick Mäder, and Marco Seeland. 2022. PRECODE - A Generic Model Extension to Prevent Deep Gradient Leakage. In *IEEE/CVF Winter Conference on Applications of Computer Vision, WACV 2022, Waikoloa, HI, USA, January 3-8, 2022*. IEEE, 3605–3614.

[44] Daniel Scheliga, Patrick Mäder, and Marco Seeland. 2023. Dropout is not all you need to prevent gradient leakage. In *Proceedings of the AAAI Conference on Artificial Intelligence*, Vol. 37. 9733–9741.

[45] Reza Shokri and Vitaly Shmatikov. 2015. Privacy-preserving deep learning. In *Proceedings of the 22nd ACM SIGSAC conference on computer and communications security*. 1310–1321.

[46] Reza Shokri, Marco Stronati, Congzheng Song, and Vitaly Shmatikov. 2017. Membership inference attacks against machine learning models. In *2017 IEEE Symposium on Security and Privacy (SP)*. IEEE, 3–18.

[47] Connor Shorten and Taghi M Khoshgoftaar. 2019. A survey on image data augmentation for deep learning. *Journal of big data* 6, 1 (2019), 1–48.

[48] Aleksei Triastcyn and Boi Faltings. 2020. Federated generative privacy. *IEEE Intelligent Systems* 35, 4 (2020), 50–57.

[49] Stacey Truex, Nathalie Baracaldo, Ali Anwar, Thomas Steinke, Heiko Ludwig, Rui Zhang, and Yi Zhou. 2019. A hybrid approach to privacy-preserving federated learning. In *Proceedings of the 12th ACM workshop on artificial intelligence and security*. 1–11.

[50] Joost Van Amersfoort, Lewis Smith, Yee Whye Teh, and Yarin Gal. 2020. Uncertainty estimation using a single deep deterministic neural network. In *International conference on machine learning*. PMLR, 9690–9700.

[51] Tianhao Wang, Yuheng Zhang, and Ruoxi Jia. 2021. Improving robustness to model inversion attacks via mutual information regularization. In *Proceedings of the AAAI Conference on Artificial Intelligence*, Vol. 35. 11666–11673.

[52] Zhou Wang, Alan C Bovik, Hamid R Sheikh, and Eero P Simoncelli. 2004. Image quality assessment: from error visibility to structural similarity. *IEEE transactions on image processing* 13, 4 (2004), 600–612.

[53] Zhibo Wang, Yuting Huang, Mengkai Song, Libing Wu, Feng Xue, and Kui Ren. 2022. Poisoning-assisted property inference attack against federated learning. *IEEE Transactions on Dependable and Secure Computing* (2022).

[54] Zhibo Wang, Mengkai Song, Zhibei Zhang, Yang Song, Qian Wang, and Hairong Qi. 2019. Beyond inferring class representatives: User-level privacy leakage from federated learning. In *IEEE INFOCOM 2019-IEEE Conference on Computer Communications*. IEEE, 2512–2520.

[55] Wenqi Wei, Ling Liu, Margaret Loper, Ka-Ho Chow, Mehmet Emre Gursoy, Stacey Truex, and Yanzhao Wu. 2020. A framework for evaluating client privacy leakages in federated learning. In *Computer Security-ESORICS 2020: 25th European Symposium on Research in Computer Security, ESORICS 2020, Guildford, UK, September 14–18, 2020, Proceedings, Part I* 25. Springer, 545–566.

[56] Xi Wu, Matthew Fredrikson, Somesh Jha, and Jeffrey F. Naughton. 2016. A Methodology for Formalizing Model-Inversion Attacks. In *IEEE 29th Computer Security Foundations Symposium, CSF 2016, Lisbon, Portugal, June 27 - July 1, 2016*. IEEE Computer Society, 355–370.

[57] Yuncheng Wu, Shaofeng Cai, Xiaokui Xiao, Gang Chen, and Beng Chin Ooi. 2020. Privacy Preserving Vertical Federated Learning for Tree-based Models. *Proc. VLDB Endow.* 13, 11 (2020), 2090–2103.

[58] Chaowei Xiao, Bo Li, Jun-Yan Zhu, Warren He, Mingyan Liu, and Dawn Song. 2018. Generating Adversarial Examples with Adversarial Networks. In *Proceedings of the Twenty-Seventh International Joint Conference on Artificial Intelligence, IJCAI 2018, July 13-19, 2018, Stockholm, Sweden*. ijcai.org, 3905–3911.

[59] Han Xiao, Kashif Rasul, and Roland Vollgraf. 2017. Fashion-mnist: a novel image dataset for benchmarking machine learning algorithms. *arXiv preprint arXiv:1708.07747* (2017).

[60] Xiaokui Xiao, Guozhang Wang, and Johannes Gehrke. 2010. Differential privacy via wavelet transforms. *IEEE Transactions on knowledge and data engineering* 23, 8 (2010), 1200–1214.

[61] LeCun Yann, Cortes Corinna, and J.C. Burges Christopher. 1998. THE MNIST DATABASE of handwritten digits. <http://yann.lecun.com/exdb/mnist/>. Online; accessed 28-July-2024.

[62] Jason Yosinski, Jeff Clune, Yoshua Bengio, and Hod Lipson. 2014. How Transferable Are Features in Deep Neural Networks?. In *Proceedings of the 27th International Conference on Neural Information Processing Systems - Volume 2* (Montreal, Canada) (NIPS’14). MIT Press, Cambridge, MA, USA, 3320–3328.

[63] Ashkan Yousefpour, Igor Shilov, Alexandre Sablayrolles, Davide Testuggine, Karthik Prasad, Mani Malek, John Nguyen, Sayan Ghosh, Akash Bharadwaj, Jessica Zhao, et al. 2021. Opacus: User-friendly differential privacy library in PyTorch. *arXiv preprint arXiv:2109.12298* (2021).

[64] Chengliang Zhang, Suyi Li, Junzhe Xia, Wei Wang, Feng Yan, and Yang Liu. 2020. {BatchCrypt}: Efficient homomorphic encryption for {Cross-Silo} federated learning. In *2020 USENIX annual technical conference (USENIX ATC 20)*. 493–506.

[65] Hongyi Zhang, Moustapha Cissé, Yann N. Dauphin, and David Lopez-Paz. 2018. mixup: Beyond Empirical Risk Minimization. In *6th International Conference on Learning Representations, ICLR 2018, Vancouver, BC, Canada, April 30 - May 3, 2018, Conference Track Proceedings*. OpenReview.net.

[66] Xinwei Zhang, Xiangyi Chen, Mingyi Hong, Zhiwei Steven Wu, and Jinfeng Yi. 2022. Understanding clipping for federated learning: Convergence and client-level differential privacy. In *International Conference on Machine Learning, ICML 2022*.

[67] Yuheng Zhang, Ruoxi Jia, Hengzhi Pei, Wenxiao Wang, Bo Li, and Dawn Song. 2020. The secret revealer: Generative model-inversion attacks against deep neural networks. In *Proceedings of the IEEE/CVF conference on computer vision and pattern recognition*. 253–261.

[68] Xuejun Zhao, Wencan Zhang, Xiaokui Xiao, and Brian Lim. 2021. Exploiting explanations for model inversion attacks. In *Proceedings of the IEEE/CVF International Conference on Computer Vision*. 682–692.

[69] Ligeng Zhu, Zhijian Liu, and Song Han. 2019. Deep Leakage from Gradients. In *Advances in Neural Information Processing Systems 32: Annual Conference on Neural Information Processing Systems 2019, NeurIPS 2019, December 8-14, 2019, Vancouver, BC, Canada*. 14747–14756.

[70] Peifei Zhu, Genki Osada, Hirokatsu Kataoka, and Tsubasa Takahashi. 2023. Frequency-aware GAN for adversarial manipulation generation. In *Proceedings of the IEEE/CVF international conference on computer vision*. 4315–4324.

[71] Yuanxin Zhuang, Chuan Shi, Mengmei Zhang, Jinghui Chen, Lingjuan Lyu, Pan Zhou, and Lichao Sun. 2024. Unveiling the Secrets without Data: Can Graph Neural Networks Be Exploited through Data-Free Model Extraction Attacks?. In *33rd USENIX Security Symposium, USENIX Security 2024, Philadelphia, PA, USA, August 14-16, 2024*. USENIX Association.

A APPENDIX

A.1 Detailed Model Structures

In this section, We introduce the details of the GAN models and the federated classifier. Let N_{out} denote the number of feature maps output by each layer. For both the *attacker’s* and *defender’s generator*, we adopt the same architecture, as outlined in Table 4. It is worth noting that the input layer’s N_{out} corresponds to the concatenation of a Gaussian noise vector with 100 elements and a label embedding with 10 elements. The architecture of the *defender’s discriminator* is presented in Table 5. Here, $C(x)$ represents a set of 64 feature maps. We augment the label embedding to match the size of $C(x)$ and subsequently concatenate them to serve as the input for the defender’s discriminator. As for the *federated model*, its architecture is provided in Table 6. In the GAN-based attack [17], the adversary can construct the discriminator of the attacking GAN by expanding the output dimension of the federated model from 10 to 11. The additional class is utilized to classify the fake images.

Table 4. The generator architecture used in both the defender’s and attacker’s GAN models. N_{out} denotes the number of feature maps output by each layer.

Layer	Name	N_{out}	Function
0	Input	110	Noises and labels
1	ConvTranspose2d	256	Kernel 4×4
2	BatchNorm2d	256	Batch normalization
3	ReLU	256	Activation
4	ConvTranspose2d	128	Kernel 4×4
5	BatchNorm2d	128	Batch normalization
6	ReLU	128	Activation
7	ConvTranspose2d	64	Kernel 4×4
8	BatchNorm2d	64	Batch normalization
9	ReLU	64	Activation
10	ConvTranspose2d	3	Kernel 4×4
11	Tanh	3	Activation

Table 5. The discriminator architecture used in the defender’s GAN model. The negative slope used in leaky ReLU is 0.2.

Layer	Name	N_{out}	Function
0	Input	128	$C(x)$ and labels
1	Conv2d	128	Kernel 4×4
2	InstanceNorm2d	128	Instance normalization
3	LeakyReLU	128	Activation
4	Conv2d	256	Kernel 4×4
5	InstanceNorm2d	256	Instance normalization
6	LeakyReLU	256	Activation
7	Conv2d	512	Kernel 4×4
8	InstanceNorm2d	512	Instance normalization
9	LeakyReLU	512	Activation
10	Conv2d	1	Kernel 4×4

Table 6. The architecture of the federated model. By changing N_{out} of the final layer from 10 to 11 (the additional class is for fake images), we can use the federated model as the discriminator of the attacker’s GAN model [17].

Layer	Name	N_{out}	Function
0	Input	3	Input image
1	Conv2d	16	Kernel 3×3
2	ReLU	16	Activation
3	MaxPool2d	16	Kernel 2×2
4	Conv2d	64	Kernel 3×3
5	ReLU	64	Activation
6	MaxPool2d	64	Kernel 2×2
7	Dropout	64	Rate 0.5
8	Linear	100	Dense Layer
9	ReLU	100	Activation
10	Linear	10	Dense Layer